Molecular One- and Two-Qubit Systems with Very Long Coherence Times

Dennis Schäfter, Jonathan Wischnat, Lorenzo Tesi, J. Alejandro De Sousa, Edmund Little, Jake McGuire, Marta Mas-Torrent, Concepció Rovira, Jaume Veciana, Floriana Tuna, Núria Crivillers, and Joris van Slageren*

General-purpose quantum computation and quantum simulation require multi-qubit architectures with precisely defined, robust interqubit interactions, coupled with local addressability. This is an unsolved challenge, primarily due to scalability issues. These issues often derive from poor control over interqubit interactions. Molecular systems are promising materials for the realization of large-scale quantum architectures, due to their high degree of positionability and the possibility to precisely tailor interqubit interactions. The simplest quantum architecture is the two-qubit system, with which quantum gate operations can be implemented. To be viable, a two-qubit system must possess long coherence times, the interqubit interaction must be well defined and the two qubits must also be addressable individually within the same quantum manipulation sequence. Here results are presented on the investigation of the spin dynamics of chlorinated triphenylmethyl organic radicals, in particular the perchlorotriphenylmethyl (PTM) radical, a mono-functionalized PTM, and a biradical PTM dimer. Extraordinarily long ensemble coherence times up to 148 µs are found at all temperatures below 100 K. Two-qubit and, importantly, individual qubit addressability in the biradical system are demonstrated. These results underline the potential of molecular materials for the development of quantum architectures.

1. Introduction

Quantum technologies appear to be on the threshold of crossing from the laboratory to real application: Space-based quantum key distribution now allows quantum communication between ground stations that are a thousand kilometers apart,[1] quantum processors now feature hundreds of qubits,[2] and quantum sensors have been used to record the action potential of single neurons in a living organism,[3] Yet, in spite of this impressive progress, many non-trivial hurdles remain to be overcome. For example, superconducting transmon quantum bits (qubits) are close to practical application, but operate at millikelvin temperatures, and their macroscopic size and individual shielded wiring requirement fundamentally limit their scalability. The rightly much celebrated nitrogen-vacancy (NV$^-$) centers in diamond possess much less impressive coherence properties when located close (<10 nm) to the diamond surface,[4] and multi-qubit arrays with deterministic inter-qubit couplings have not been prepared thus far.[5]

Molecules could solve some of such limitations since they possess properties that make them potentially very interesting for quantum applications: i) Their physicochemical properties are extensively tunable by chemical synthetic means,[6] ii) they are highly monodisperse with sizes at the nanoscale or even lower, iii) their production is scalable, iv) they possess intrinsically non-harmonic energy spectra

D. Schäfter, J. Wischnat, L. Tesi, J. McGuire, J. van Slageren
Institute of Physical Chemistry and Center for Integrated Quantum Science and Technology
University of Stuttgart
Pfaffenwaldring 55, 70569 Stuttgart, Germany
E-mail: slageren@ipc.uni-stuttgart.de

J. A. De Sousa, M. Mas-Torrent, C. Rovira, J. Veciana, N. Crivillers
Institut de Ciència de Materials de Barcelona (ICMAB-CSIC)
Networking Research Center on Bioengineering Biomaterials and Nanomedicine (CIBER-BBN)
Campus de la UAB
Bellaterra 08193, Spain

J. A. De Sousa
Laboratorio de Electroquímica
Departamento de Química
Facultad de Ciencias
Universidad de los Andes
Mérida 5101, Venezuela

E. Little, F. Tuna
Department of Chemistry and Photon Science Institute
The University of Manchester
Oxford Road, Manchester M13 9PL, UK

allowing preparation of multiple-state coherences,[7] and v) they can be arranged in highly ordered 2D and 3D arrays,[8,9] allowing the exploitation of the dipolar interaction to implement more-qubit operations. The quintessential figure of merit for any qubit implementation in quantum computing is the ratio of coherence time (the time available to complete a quantum algorithm) to the single gate operation time.[10] For microwave-manipulated spin qubits, the 90 degree pulse time, that is, the microwave irradiation time required to generate a coherent superposition state with equal contributions of the |0> and |1> levels, is typically used as a measure for the single gate operation time. Furthermore, the sensitivity of quantum sensing of magnetic fields is ultimately limited by the quantum coherence time of the qubits.[4] In experiments on ensembles of qubits, a lower bound estimate of the quantum coherence time, typically denoted phase memory time is obtained (usually by Hahn echo measurements, see below). Molecular qubits (MQBs) have reached ensemble phase memory times up to the millisecond range at double digit Kelvin temperatures,[11] making them competitive with other spin qubits in this respect (**Table 1**).[12] One drawback of MQBs is that single entity readout of these species is a little explored subject, in spite of the fact that single entity electrical readout of MQBs has been achieved,[13] and optical single-entity readout appears to be around the corner.[14,15]

Exploiting the atomic-scale placement position of MQBs, a number of potential two- and more qubit systems have been developed. In one approach, systems are used that possess interqubit interactions that are stronger than experimental single-qubit rotation rates (nutation or Rabi rotation rates). Two-qubit levels are then encoded in coupled states of the dimer, and microwave induced transitions in the coupled system can be mapped onto typical quantum gate operations, such as CNOT.[16,17] More operational flexibility is afforded when the inter-qubit interaction is small compared to the single qubit rotation time corresponding to typical 90 degree pulse times of 10 ns, because this allows for single-qubit rotations in addition to two-qubit operations. Thus, the full CNOT gate operation actually corresponds to the transformation $U_{CNOT} = \sqrt{i}\, Z_1 \bar{Z}_2 X_2 U_J(\frac{1}{2}J) Y_2$, where X, Y, Z are single qubit rotations, 1 and 2 are control and target qubits, respectively, and U_J is the time evolution operator corresponding to the inter-qubit interaction J, that is, the two-qubit part of the gate operation.[18] For two-qubit systems with pure magnetic-dipolar inter-qubit interactions, this weak interaction requirement translates to minimal inter-qubit distances of 1.6–1.8 nm. These distances must be well defined and fixed to avoid distributions in and modulation of the inter-qubit interaction. It is noteworthy that the latter point is easily attained in MQBs by the flexibility of molecular synthesis allowing the control of the relative arrangement of qubits modifying their inter-qubit interactions through the bridge linking the qubits. A number of systems with two or more weakly coupled spin centers have thus been proposed as two- and more-qubit implementations (Table 1).[19,20] Interestingly, systems that fulfill the above criteria have also been studied extensively as model systems for distance determinations in structural biology.[21–23] In the latter type of studies, the phase memory times that are so critical for quantum applications are unfortunately typically not reported.

Most investigations into MQBs have focused on simple mononuclear metal complexes, since it was quickly realized that
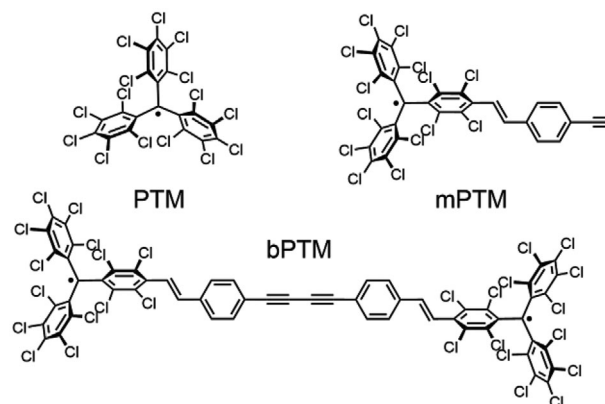

Figure 1. Chemical structures of the three studied compounds PTM, mPTM, and bPTM.

these possess much longer coherence times than the exchange-coupled clusters studied initially.[12] The second realization was that the nuclear spins of the hydrogen atoms of the ligands were the main cause for decoherence in MQBs and that removal of such hydrogen atoms improved coherence times.[11,24] In fact, hydrogen-less $N@C_{60}$ displays very long coherence times, and has been studied in detail at the single-qubit level.[7,25] However, the preparation of pure material is exceedingly tedious,[26] functionalization is challenging, and indeed potential two-qubit systems based on bis-$N@C_{60}$-compounds have not been synthesized in significant quantities, as far as we are aware.[27] Persistent neutral organic radicals such as substituted triarylmethyl or 2,2,6,6-tetramethylpiperidinyloxyl (TEMPO), on the other hand, have been extensively investigated for their use in site-directed spin labeling, which allows determining distances in biological systems in physiologically relevant conditions or even in intact cells.[28] Such organic radicals have been much less investigated in the context of quantum applications, even though phase memory times of up to 13 μs have been reported (Table 1). Similar hydrogen removal strategies (by deuteration) as for transition metal complexes have been pursued especially in the case of TEMPO and tris(tetrathioaryl)methyl (TthAM) radicals. Because of their weak spin-orbit coupling, organic radicals tend to feature much smaller anisotropies, leading to narrower electron paramagnetic resonance (EPR) spectra in randomly oriented samples such as powder or frozen solutions. Consequently, in bulk measurements, a much larger fraction of the ensemble is addressed for a given excitation bandwidth in the case of fully organic MQBs than for metal complex based MQBs. The fact that the spectral widths are narrower for organic radicals than for metal complexes might be thought a drawback for two- and more qubit systems, because quantum gate operations require individual spectral addressability of the different qubits. However, if the excitation frequencies of the qubits differ too much, they can easily exceed source and resonator bandwidths, precluding quantum gate operations. In fact, narrow lines can be a distinct advantage to ensure individual addressability of qubits in more-qubit systems beyond two-qubit ones.

Here we focus on chlorinated triphenylmethyl organic radicals (**Figure 1**) that feature EPR spectra with very narrow lines, as potential molecular one- and two-qubit systems. We show that

Table 1. Experimentally determined ensemble low-temperature phase memory times (T_M) for selected monomeric and dimeric molecular qubits (MQBs). For the monomers, organic MQBs have been highlighted in bold font, while for the dimeric ones, those examples for which a coherent measurement addressing the inter-qubit interaction has been performed, have been highlighted in the same manner.

Monomeric MQBs				
MQB1[a]	MQB2[a]	Bridge[b]	T_M [µs]	Ref.
$[V(dbddto)_3]^{2-}$	–	–	675	[11]
Graphenoid	–	–	290	[30]
$N@C_{60}$	–	–	230	[31]
PTM	–	–	148	This work
mPTM	–	–	114	This work
$[Cu(mnt)_2]^{2-}$	–	–	68	[24]
CuPc	–	–	41	[32]
[CpTi(cot)]	–	–	34	[33]
$[Cu(dbm)_2]$	–	–	25	[34]
$[Au^{III}(adt_2^{3-})]$	–	–	21	[35]
TEMPO-SAM	–	–	13.5	[36]
PTM	–	–	13	[29]
Blatter	–	–	7.8	[37]
Triplet C60	–	–	6.2	[38]
NitSAc	–	–	5.41	[39]
TthAM	–	–	5.1	[40]
dpph	–	–	3.9	[41]
TEMPO	–	–	3.2	[42]
CTPO	–	–	2.79	[39]
BDPA	–	–	2.3	[43]

Dimeric MQBs				
PTM	PTM	*lr/c*	67	This work
CuPor	TiCp	*lr/c*	20.77, 8.20	[14]
TthAM	**triplet C60**	*sf/nc*	2.2, 6.2	[38]
CuZnHPDK	CuZnHPDK	*lr/c*	6.03	[44]
VO(TrPP)	VO(TrPP)	*sr/c*	5.8	[45]
VO(fTrPP)	VO(fTrPP)	*sr/c*	5.5	[46]
CuNiHPDK	CuNiHPDK	*lr/c*	3.59	[44]
MnDOTA	**MnDOTA**	*lr/nc*	5.9	[47]
TthAM	**TEMPO**	*sf/nc*	3.8	[48]
TthAM	**TthAM**	*lr/c*	3.3	[49]
Cr7Ni	**Cr7Ni**	*lr/nc*	3.239	[20]
Y@C82	**Y@C82**	*lr/nc*	2	[50]
GdPyMTA	**GdPyMTA**	*lr/c*	1.4	[51]
TEMPO	**Mn-tpy**	*lr/c*	1.0	[52]
VOCat	VOCat	*sr/nc*	1	[53]
Cu	Cu7Ni	*lr/nc*	1, 0.6	[54]
VO-ON	VO-ON	*sr/c*	0.26	[55]

[a] Abbreviations of spin containing units of MQBs: dbddto: 2,5-dithioxobenzo[1,2-d:3,4-d']bis[1,3]dithio-lene-7.8-dithiolate; mnt: maleonitriledithiolate, (Z)-1,2-dicyanoethene-1,2-bis(thiolate); Pc: phthalocyaninate anion; cot: 1,3,5,7-cyclooctatetraene; dbm: dibenzoylmethane anion, 1,3-diphenylpropane-1,3-dionate; adt: bis(p-anisyl)-1,2-ethenedithiolate; Nit: nitronyl nitroxide radical; TthAM: tri(tetrathioaryl)methyl radical; dpph: 2,2-diphenyl-1-picrylhydrazyl radical; TEMPO: (2,2,6,6-Tetramethylpiperidin-1-yl)oxyl; CTPO: 3-carbamoyl-2,2,5,5-tetramethyl-1-pyrrolidinyloxy radical; BDPA: 1,3-bisdiphenylene-2-phenylallyl; PTM: perchlorotriphenylmethyl radical; TTP: 5,10,15,20-tetratolylporphyrin; TrPP: 5,10,15-triphenylporphyrin; fTrPP: fused-bis-5,10,15-triphenylporphyrin; [b] Structural and electronic characteristics of bridges of dimeric MQBs: *l*, long; *s*, short; *r*, rigid; *f*, flexible, *c*, conjugated; *nc*, non-conjugated.

**ADVANCED
SCIENCE NEWS**

www.advancedsciencenews.com

**ADVANCED
MATERIALS**

www.advmat.de

Table 2. ESE-derived *g*-values and comparison with pulsed/CW EPR measurements from literature. *G*-Tensor values are reported as $10^3 (g_{1,2,3} - 2)$, $10^3 \Delta g = 10^3 (g_3 - g_1)$.

Radicals	$g_1 - 2$	$g_2 - 2$	$g_3 - 2$	$10^3 \Delta g$	Ref.
PTM	2.3(2)	2.6(2)	5.6(2)	3.3(3)	This work
mPTM	1.8(2)	2.5(2)	5.4(2)	3.6(3)	This work
bPTM	2.4(2)	2.7(2)	4.6(2)	2.2(3)	This work
PTM-CO$_2^-$	1.3	1.6	4.2	2.9	[59]
PTM-CO$_2^-$	1.5	1.5	4.0	2.5	[60]
PTM-CO$_2^-$	0.9	0.9	4.0	3.1	[61]
PTM-CO$_2$Na	1.76	2.36	4.1	2.34	[62]
PTM-CO$_2$Na	0.02	0.74	3.38	3.36	[63]
PTM-CO$_2$Na	0.05	0.05	2.71	2.66	[56]
PTM-CO$_2$H	1.32	1.68	4.29	2.97	[62]
PTM-CO$_2$Et	1.25	1.56	4.58	3.33	[62]
FT[a]	2.33	3.01	3.39	1.06	[62]

[a] Finland Trityl, which is a TthAM-type radical.[64]

replacement of all hydrogens by chlorine atoms, yielding the perchlorotriphenylmethyl (**PTM**) radical, increases the phase memory time (T_M) to an unprecedented value of 148 µs in CS$_2$, improving the previous published results (see Table 1) obtained in frozen toluene-d8.[29] Furthermore we show that the substitution of one of its chlorine atoms of the *para* position of a phenyl ring with a π-conjugated substituent containing H atoms, namely vinylenephenylene-yne, only results in a slight decrease of T_M down to 114 µs of the resulting radical, named here as the mono-functionalized PTM (**mPTM**) (Figure 1). Furthermore, we carry out pulsed dipolar spectroscopic measurements that can be thought of as the core of a true quantum gate operation such as CNOT, on a weakly coupled biradical, hereafter named **bPTM** (Figure 1). **bPTM** features a long, rigid, and π-conjugated oligoyne bridge stabilized by the PTM moieties acting as end-capping units, and still possesses a remarkably long phase memory time of 67 µs. The measurements demonstrate the suitability of this biradical as a two-qubit system for quantum gate operations.

2. Results and Discussion

Figure 1 displays the chemical structure of the three compounds investigated in this study. First of all, we investigate the well-known perchlorotriphenylmethyl radical (**PTM**). Second, we focus on evaluating the impact on the spin dynamics in radical **mPTM** produced by the replacement of a chlorine atom at the *para* position by a π-conjugated, hydrogen-containing substituent and, finally, we study the spin dynamics of the biradical (**bPTM**). The **bPTM** biradical could be considered a potential two-qubit system, as we assess in this work.

2.1. Pulsed EPR: Electron-Spin-Echo Detected Spectra

As a first step toward assessing the suitability of the three title compounds for quantum technological purposes, we have recorded electron-spin-echo-detected (ESE) Q-band (35.000 GHz)

spectra of the compounds in frozen, nuclear-spin-free CS$_2$ solution at 7 K (**Figure 2**). The fact that a clear Hahn echo is observed already indicates measurable coherence times for the three investigated radical systems revealing that they are potential MQBs. *g*-Values very close to the free electron value of $g_e = 2.00232$ are found for the three studied radicals, which agrees very well with values reported in literature for other substituted derivatives of
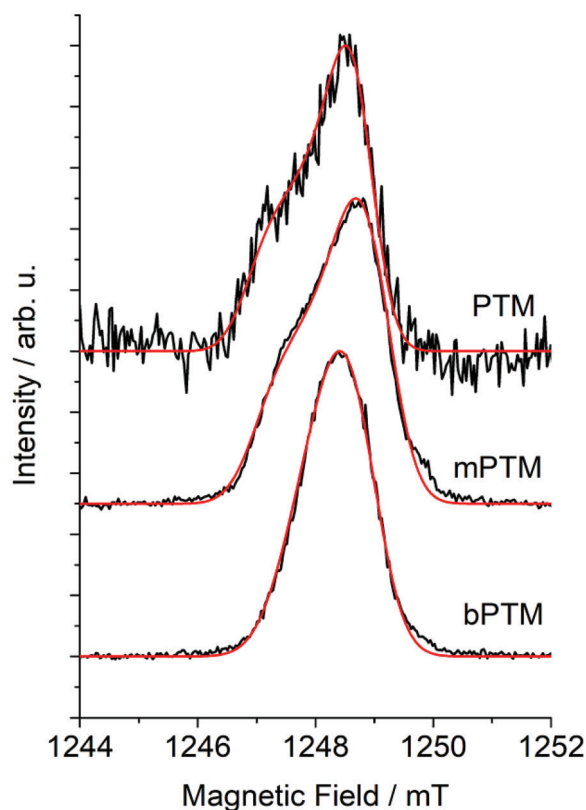

Figure 2. Q-Band electron-spin-echo-(ESE) detected spectrum of 200 µM solutions of PTM, mPTM, and bTM in CS$_2$ at 7 K.

**ADVANCED
SCIENCE NEWS**

www.advancedsciencenews.com

**ADVANCED
MATERIALS**

www.advmat.de

the **PTM** radical (**Table 2** and Table S1, Supporting Information). The spectra reveal a small but significant *g*-value anisotropy (defined as the difference between maximum and minimum values of the *g*-tensor components, Table 2), which varies a little along the series, but this is hardly significant. The smallest *g*-value anisotropy is found for **bPTM** and indeed this value is the smallest one reported for substituted **PTM** radicals that we are aware of. The *g*-value anisotropy of these **PTM** radicals is larger than that found for TthAM-type trityl radicals (Table 2 and Table S1, Supporting Information), which was attributed to the relatively large spin–orbit coupling of the chlorine substituents.[56] Chlorine has a nuclear spin of $I = 3/2$, and experimental and calculated values of chlorine hyperfine coupling constants in PTM-type radicals amount to several MHz.[56–58] Potentially, hyperfine interaction between the electron spin and the large number of chlorine nuclear spins could influence the quantum coherence properties of the PTM radicals. However, no hyperfine coupling between the electron spin and the chlorine nuclear spin is resolved in the spectra. This is because first, the spin density is largely located on the central carbon atom, and hyperfine couplings are therefore weak. Second, because of the fast relaxation of quadrupolar chlorine nuclei, any interaction with the electron spin is averaged to zero.[57] To assess whether some of the line broadening is due to unresolved chlorine hyperfine splitting and if at the lowest temperature, the dynamics of the latter might slow down to the point where it may influence the electron spin coherence, we investigated the temperature dependence of the ESE spectra. To this end, we investigated solid state samples rather than frozen solutions to extend the accessible temperature range beyond the melting point of the solvent. First, we investigated a sample of **PTM** in poly(bisphenol-A sulfone, PSF) (Figure S1, Supporting Information), where the room temperature spectrum could be fitted considering anisotropic inhomogeneous broadening, modeled as *g*-strain. This results in *x*- and *z*-linewidths (FWHM) of ≈3 MHz and a *y*-linewidth that is twice as much (6.2 MHz). Upon lowering the temperature, the *x*-linewidth remains essentially constant, the *z*-linewidth increases slightly, but the *y*-linewidth increases strongly and reaches 16.6 MHz at 7 K (Figure S2, Supporting Information). To elucidate if this feature is particular to this sample, we have also studied **mPTM** doped at the 0.1% level into its diamagnetic synthetic precursor triphenylmethane derivative (**αH-mPTM**, Figure S3, Supporting Information). Indeed, also in this case, a clear difference between the room temperature and low-temperature spectra is seen. We hypothesize that this difference may be due to hyperfine coupling to the chlorine nuclei: At high temperatures, the chlorine nuclear spin dynamics is too fast to influence the EPR spectra, while at low temperatures it leads to (unresolved) hyperfine splitting. Unfortunately, the Hilbert space dimension of one electron spin coupling to up to 15 chlorine nuclear spins (2×10^9) precludes simulating the entire system by means of existing EPR simulation tools.

2.2. Pulsed EPR: Spin Dynamics

By varying the interpulse delay time in the Hahn echo sequence, the phase memory time can be determined. In dilute conditions, the decoherence mechanism typically involves nuclear-spin flip-flop processes leading to spectral diffusion.[34] Due to the strong nuclear magnetic moment of protons, it is especially advantageous to remove hydrogen atoms as much as possible from the sample. In the case of the three studied radical compounds, this has to a large extent already been achieved by their perchlorination. For the same reason, we use the largely nuclear-spin free CS_2 solvent to prepare frozen solution samples. The Hahn echo decay as function of interpulse delay time measured on a frozen solution sample of **PTM** in CS_2 (Figure S4, Supporting Information) can be fitted by means of a biexponential decay function $I(2\tau) = A_f \exp(-\frac{2\tau_f}{T_{Mf}}) + A_1 \exp(-\frac{2\tau_s}{T_{Ms}})$, that is, the sum of fast (*f*) and slow (*s*) decoherence processes. Such biexponential decays have been observed before for frozen solutions of copper(II) diketonates, where the relative contributions of fast and slow relaxation processes depend on the exact glassing conditions.[34] In fact, CS_2 is a rather poor solvent for low-temperature studies, since it does not form good solvent glasses.[31] Here we follow literature, and attribute the slower process to T_M and the faster process to spectral diffusion due to locally enhanced concentration.[65] Astoundingly, the phase memory time for the **PTM** radical in CS_2 at 7 K thus extracted is $T_M = 123(47)$ μs. This phase memory time is much larger than that of any other triarylmethyl radicals, including the intensely studied TthAM-type radicals such as **OX63** and **Finland Trityl** radicals, which have phase memory times of not more than ≈5 μs in low-temperature frozen solutions. Phase memory times are also longer than for chlorinated trityl radicals in solvents with nuclear spins, which feature phase memory times of up to 13.3 μs (Table 1). We attribute this long coherence time to the virtual removal of proton and deuterium nuclear spins from both the compound and the matrix, a strategy that has proven very fruitful in transition metal complexes studies.[11,24] In fact, this coherence time propels **PTM** to fourth place in the ranking of phase memory times of molecular systems after $[V(dbddto)_3]^{2-}$ ($T_M = 675$ μs), graphenoids ($T_M = 290$ μs), and N@C60 ($T_M = 230$ μs), all in CS_2 (Table 1). Upon heating the sample, the phase memory time remains constant within experimental error up to 50 K (the maximum is $T_M = 148(39)$ at 50 K), and only decreases slightly beyond that temperature (**Figure 3** and Table S2, Supporting Information). Apparently therefore, if there is any change in the chlorine spin dynamics, it does not adversely influence the phase memory time.

To be able to incorporate PTM radical derivatives into quantum technological devices, or to prepare multi-qubit systems, the PTM unit must be functionalized, as in **mPTM** (Figure 1). In literature, this functionalization has been used to great effect to immobilize PTM species on metallic and oxide surfaces, including further functionalization yielding multistate electrochemical switches.[66] The terminal alkyne as well as the vinylenephenyleneyne bridge of the **mPTM** radical feature some hydrogen atoms, and the question is then how this influences the phase memory time. Hahn echo measurements (Figure S5, Supporting Information) reveal only very slightly lower phase memory times for **mPTM** than for **PTM** itself (Figure 3 and Table S3, Supporting Information), with the maximum value of $T_M = 114(14)$ at 30 K. This finding has enormous implications for the use of MQBs in quantum technologies and establishes **mPTM** as a versatile building block for such technologies since it can be grafted on Au or Si surfaces to provide ordered arrays for
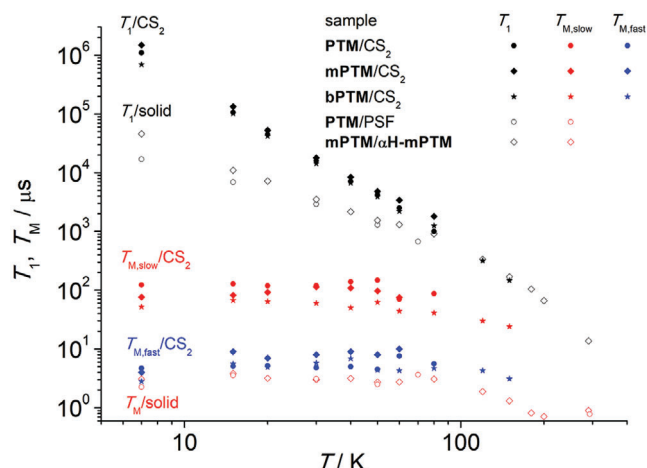
ADVANCED
SCIENCE NEWS
www.advancedsciencenews.com

ADVANCED
MATERIALS
www.advmat.de

Figure 3. Spin dynamics times extracted from fits of the echo decay curves recorded on CS_2 frozen solution (filled symbols) or solid state (open symbols) samples of PTM (circles), mPTM (squares), and dPTM (stars). T_1 (black symbols) times were obtained from monoexponential fits, solution T_M times from biexponential fits with the slow component in red and the fast component in blue. For the solid state samples of PTM in PSF polymer and mPTM in αH-mPTM, T_M times were determined by monoexponential fits.

future quantum technologies. To go a step further, we have investigated the phase memory time and its temperature dependence (Figure S6, Supporting Information) of the **bPTM** species, which is a potential two-qubit system. We find that the phase memory times for **bPTM** (Figure 3 and Table S4, Supporting Information) are again only a little lower, with a maximum value of $T_M = 67(9)$ at 15 K, which is very encouraging for the potential future application of PTM-based MQBs in quantum technologies. In this case, a Hahn echo signal was observed up to 150 K, that is, close to the melting point of CS_2 (160 K). Here we also note that the coherence time might be further improved by removing ^{13}C nuclear spins from the matrix.[67]

To extend the temperature range of the measurements and circumvent the limitation posed by a solvent melting, we have incorporated the studied radicals into solid matrices. Thus, we have performed Hahn-echo measurements (Figure S7, Supporting Information) on a 0.1% dispersion of **PTM** radical in PSF, revealing monoexponential echo decays with time constants that are much shorter than those obtained for the CS_2 frozen solvents (Figure 3 and Table S5, Supporting Information), in accordance with the large concentration of proton spins in the polymer sample. Similar effects have been observed in literature.[33] At room temperature, a phase memory time of 0.78(8) μs was found. **PTM** radicals are prepared by oxidative deprotonation of the corresponding triarylmethane that can serve as diamagnetic host materials for the radical species. Hence, we have prepared a sample of diamagnetic **αH-mPTM** doped with 0.1% dispersion of **mPTM** and determined phase memory times at different temperatures (Figure 3; Figure S8 and Table S6, Supporting Information). Again, these values are much lower than those found in the proton-free CS_2 matrix. Nevertheless, even at room temperature, the phase memory time for **mPTM** in **αH-mPTM** is still 0.898(4) μs (Table S7, Supporting Information).

Spin–lattice relaxation, that is, the process of energy exchange between the spin system and its surroundings and characterized by the time constant T_1. The T_1 time is the fundamental upper limit for T_M ($T_{M,max} = 2\,T_1$). To determine T_1, we have carried out inversion recovery experiments on all samples. For the frozen CS_2 solution samples at the lowest temperatures employed, T_1 is of the order of 1 s, indicating that T_M is not limited by T_1 for these samples. Upon increasing the temperature, T_1 rapidly decreases (Figure 3 and Tables S2–S4, Supporting Information). The plot of $\log(T_1)$ versus $\log(T)$ is pronouncedly linear, and the minimal model to fit the temperature dependence of T_1 therefore consists of a single Raman-like term $T_1^{-1} = CT^n$ with $n = 2.76$. Similar values of the phenomenological Raman-like exponent have been often found for T_1 relaxation of $S = \frac{1}{2}$ systems in frozen solution.[68,69] Theoretically, the Raman exponent for $S = \frac{1}{2}$ (Kramers) systems in a perfect lattice should be $n = 9$ at temperatures much lower than the Debye temperature T_D of the medium.[70,71] In practice, such an exponent is never found for glassy materials such as frozen solutions. The Raman exponent is predicted to be $n = 2$, that is, reasonably close to what we found, for temperatures much higher than the Debye temperature.[71] However, the Debye temperature for CS_2 was reported to be ≈160 K,[72] and therefore for most of the data points $T < T_D$. In case a phonon bottleneck is operative, that is, the excitation energy released by the spin system cannot spread rapidly enough throughout the lattice and hence to the surroundings, an exponent of $n = 2$ is expected.[71,73] However, in view of the dilute nature of the samples, occurrence of a phonon bottleneck is unlikely. A large number of models exist that aim to take into account the contribution of local modes to the spin–lattice relaxation.[74] Such local modes can be molecular vibrations, but also phonons that are localized on a defect in the crystal lattice and do not propagate through the lattice. Local mode models typically predict an exponential temperature dependence of the spin–lattice relaxation rate at lowest temperature.[74,75] At intermediate temperatures, for resonance mode frequencies much higher than the Debye frequency, a T^3 temperature dependence has been proposed.[74,76] Finally, at high temperatures the T^2 temperature dependence is found again.[74] Using the real phonon spectrum rather than a fictitious Debye phonon distribution has been reported to yield somewhat but not dramatically better agreement between experiment and simulation.[77] From the foregoing, the local mode-assisted relaxation scenario in the intermediate temperature regime would appear most reasonable. However, simulations based on such a model, that is, considering the formula $T_1^{-1} \propto \exp(\Delta_{loc}/T)/(\exp(\Delta_{loc}/T) - 1)^2$ do not yield an acceptable fit of the experimental data (Figure S9, Supporting Information). Clearly, the situation is more complicated and perhaps several local modes in the solvent and in the molecule must be taken into account. This is in contrast with literature reports on T_1 relaxation in other polychlorinated triphenylmethyl radicals, where a combination of high-value exponent Raman-like relaxation and local mode relaxation was used.[59,78] The strong similarity between the three PTM radical compounds studied suggests that molecular local mode vibrations outside of the triarylmethane core, that is, those that involve the vinylenephenylenediyne bridge do not play a significant role in spin–lattice relaxation. To further investigate this issue, we carried out quantum chemical DFT calculations on both monoradicals. Structure

optimizations gave stable equilibrium structures (Figures S10 and S11, Supporting Information and Tables S8 and S9, Supporting Information). Calculations of the vibrational spectra (Tables S10 and S11 and Figures S12 and S13, Supporting Information) reveal a number of low-frequency vibrational modes of comparable energies corroborating the hypothesis that similar local modes govern the relaxation of these two radicals.

Finally, we measured T_1 relaxation times for **PTM** in PSF and **mPTM** in **αH-mPTM**. Intriguingly, the T_1 temperature dependence for **mPTM** in **αH-mPTM** displays two rather distinct, but both linear temperature-dependencies below and above $\approx$100 K. In the latter range, the slope on a log–log plot is very similar to that found for the CS_2 solution samples, suggesting that here it is mainly a PTM local mode that causes spin–lattice relaxation, rather than a local matrix vibration. The slope below 100 K is much lower and the T_1 relaxation rate follows a Raman-like temperature dependence according to $T_1^{-1} = CT^n$ with $n = 1.56$, which could indicate a contribution from the direct process (for which $n = 1$ is expected), where the presumably lower speed of sound in the softer medium increases the prefactor to render the direct process contribution significant.[71]

2.3. Pulsed EPR: Dipolar Spectroscopy

We now turn to the measurements to assess the viability of **bPTM** biradical as two-qubit system. For such purposes, it is, first of all, important that the coupling strength, expressed as a rate is much lower than the manipulation time of the single qubit, also expressed as a rate (nutation rate). For a typical minimal $\pi/2$ pulse length of 10 ns, the nutation rate is $\omega = 25 \times 2\pi$ MHz. Second, the coupling between qubits should be well-defined and time-independent. For magnetic-dipolar coupling between the qubits, this means that the distance between the qubits must be well defined and the bridge between the qubits rigid. The dipolar coupling strength between two unpaired electrons with distance r amounts to $52.16\ r^{-3}$ MHz, assuming the interspin axis is perpendicular to the external field. A number of EPR pulse sequences, collectively known as pulsed dipolar spectroscopy, exist to investigate dipolar coupling in well-separated spin centers. A convenient pulsed EPR experiment to assess the weak coupling between two spin centers is the RIDME pulse sequence, which stands for relaxation-induced dipolar modulation enhancement. However, this pulse sequence relies on spontaneous T_1 relaxation of one of the spin centers and measures its influence on the dynamics of the other spin center. This sequence works best for dissimilar spin centers, where one relaxes much faster than the other,[79] and it has been reported to perform poorly for trityl radicals.[80] For narrow-linewidth spin centers such as trityl radicals, single frequency pulse methods are highly suitable to determine dipolar couplings between spin centers, because these methods work best if the resonance frequency difference between the two spin centers is less than the excitation bandwidth.[23] In these sequences, both spin centers are excited at the same time. One such method is the four-pulse single-frequency technique for refocusing dipolar couplings (SIFTER).[81] This single quantum coherence pulse sequence is $(\frac{\pi}{2})_x - \tau_1 - (\pi)_x - \tau_1 - (\frac{\pi}{2})_y - \tau_2 - (\pi)_x - \tau_2 - $ echo, where the two $\frac{\pi}{2}$-pulses along different axes in the ro-
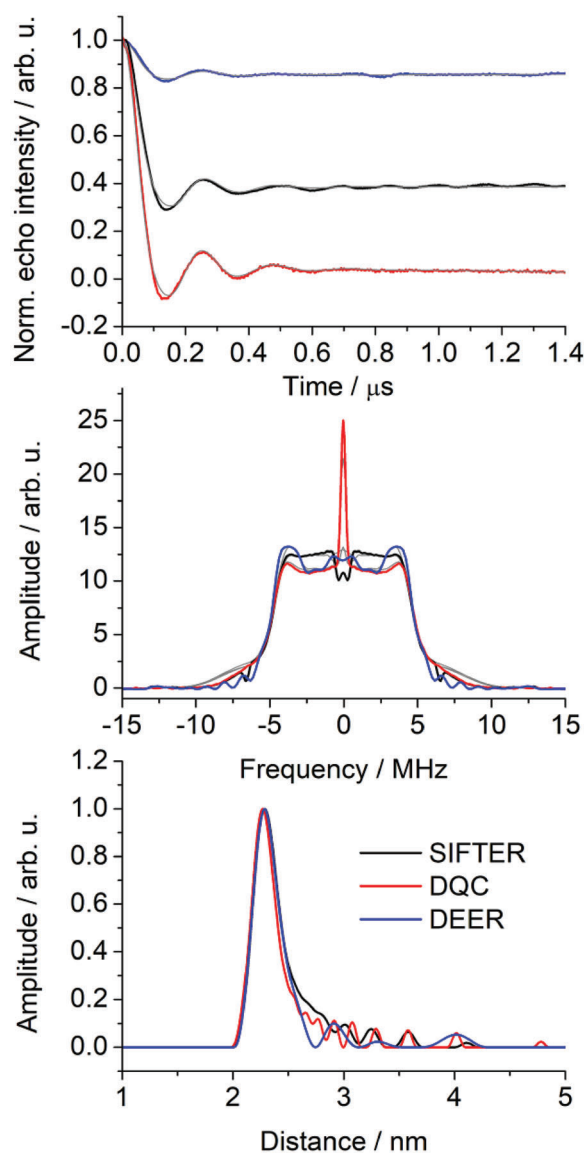

Figure 4. 4-pulse DEER (blue), SIFTER (magenta), and DQC (green) experiments performed on a 200 μM solution of bPTM in toluene:dichloromethane (1:1) performed at 34.035 GHz, 1215.4 mT (DEER)/1216.6 mT (SIFTER, DQC), and 50 K. (top) Background corrected time traces (solid lines) and simulations thereof (dotted lines) obtained using DeerAnalysis, (middle) Fourier transforms of the time traces, (bottom) distance distribution functions.

tating coordinate frame generate a solid echo (i.e., independent of relative orientation of the two dipolar-coupled spins) for $\tau_1 = \tau_2$, and the π-pulses refocus any g, A, and B-inhomogeneities. Consequently, variation of the τ_1 and τ_2 pulse delays for constant $\tau_1 + \tau_2$ gives an echo modulation that depends only on the dipolar interaction and not on decoherence. **Figure 4** shows the background corrected SIFTER measurement results for a sample of 200 μM bPTM in toluene:dichloromethane 1:1 at 50 K. The experiments display a clear signal modulation, due to the dipolar coupling between the two spin centers. The continuing oscillation to longer times is attributed to contributions from unwanted coherence

pathways. Fourier transformation of the time trace results in a clear Pake pattern, where the increased intensity around zero ν_{dip} suggests that some of the background has been falsely attributed to the intramolecular dipolar contribution. Nevertheless, distance distribution functions obtained from the time traces by means of a Tikhonov regularization fit display a clear, narrow peak centered around an inter-radical distance of 2.4 nm. Interestingly, the distance between the central carbon atoms of the PTM radical units is found to be significantly longer (2.76 nm) by means of simple force-field optimization of the structure (Figure S14, Supporting Information). This observation indicates that the effective coupling between the two radical centers is stronger than expected on the point dipole approximation and consequently the unpaired electrons are somewhat delocalized toward the bridge. In trityl radicals, the spin density is strongly localized on the methyl carbon, and the point dipole is therefore a good approximation to the magnetic moment. However, the bridge between the two spin centers is a conjugated π-system, meaning that spin exchange through the spin polarization may play a small but significant role in the effective spin-spin coupling. For short distances, that is, when the resonance frequency difference between two spins is smaller than the dipolar coupling, it has been shown that the pseudo-secular part of the dipolar coupling must be taken into account.[82] From the Fourier transformation of the time trace, a dipolar coupling of ≈4 MHz is extracted. An upper estimate of resonance frequency differences in the PTM biradical is given by the linewidth, namely, ≈2.1 mT which corresponds to 16 MHz. Hence the relevance of the pseudo-secular term in the dipolar coupling cannot be excluded here.

The description of the SIFTER experiment has assumed ideal hard pulses, that is, unity probability to affect all spins addressed by a pulse. This is typically not a bad approximation for narrow-line spectra such as those of trityl radicals. Nevertheless, imperfect pulses can lead to additional, unwanted signals, as we have seen. Such artefacts can be partially removed by appropriate phase cycling or pulse shaping.[83] A pulse sequence that specifically filters out such unwanted signals is double-quantum coherence (DQC), $(\frac{\pi}{2})_x - \tau_1 - (\pi) - \tau_1 - (\frac{\pi}{2})_x - T - (\pi) - T - (\frac{\pi}{2})_x - \tau_2 - (\pi) - \tau_2 - $ echo.[84] Here the second $\pi/2$ pulse converts first into second order coherence (double quantum coherence), which is subsequently refocused and converted back to first order antiphase coherence and to in-phase (i.e., detectable) coherence by the last π pulse. The application of an appropriate phase cycling cycle then allows separating the double quantum coherence pathway from other, undesired pathways. In the DQC measurement, T is constant, as is the sum of $\tau_1 + \tau_2$. Figure 4 displays the time traces for the DQC measurement on a frozen solution of **bPTM**. Here the echo modulation depth is clearly bigger and no spurious oscillations are observed. In the frequency domain, this corresponds to a cleaner Pake pattern and in the distance distribution function to a better defined peak without a tail toward longer distances. The sharp peak in the middle of the Pake pattern is attributed to imperfect background correction. The interspin distance obtained from this measurement is identical to that obtained from the SIFTER measurement.

The comparable results of SIFTER and DQC measurements underline the robustness of the result. However, for true quantum gate operations, the two qubits of a two-qubit system must be individually addressable. To assess this, single frequency techniques such as SIFTER and DQC that rely on broadband excitation to work are not suitable. The method of choice for individual addressing of several spin centers whilst being sensitive to spin-spin coupling is double electron-electron resonance (DEER).[85] This method employs microwave pulses of two different frequencies tuned to one or the other of the two spin centers. Importantly, because during a multipulse sequence that seeks to implement a quantum gate operation the external field cannot be changed, the two different frequencies must fall within the bandwidth of the resonator employed for the measurement.[7] For resonator Q-factors of the order of 10^2, this results in maximum frequency differences of hundreds of MHz (at Q-band) or maximum relative g-value differences of the order of 1%. This is rather small compared to differences in typical g-values for different transition metal ions, or even their g-value anisotropies, and hence an argument in favor of using stable organic radicals. Trityl radicals feature very narrow-line spectra even for organic radicals. Hence, we have carried out DEER measurements on **bPTM** to assess individual addressability of the two spin centers (symbolically denoted A and B) in this molecule. The four pulse DEER sequence $(\frac{\pi}{2})_A - \tau_1 - (\pi)_A - (\tau_1 + t) - (\pi)_B - (\tau_2 - t) - (\pi)_A - \tau_2 - $ echo is based on a constant-time refocused echo that avoids overlap between pulses.[86] A DEER time-trace (Figure 4) was obtained for **bPTM**, where the modulation depth of the time trace is clearly lower than what was observed for SIFTER and DQC, due to the selective nature of the pulses, leading to a small number of spin packets being addressed. Nevertheless, a clear oscillation is present in the time trace, which gives rise to a typical Pake pattern after phase and background corrections followed by Fourier transformation. In the distance distribution function, once more a clear peak is observed at 2.4 nm, corroborating the other pulsed dipolar spectroscopic results. From these data, we can extract the nominal two-qubit gate time as the time of the first minimum in the dipolar time trace as 140 ns, which is between the $\frac{\pi}{2}$-pulse time of 40 ns (single-qubit manipulation time) and the coherence time of $T_M = 62$ μs at 50 K (Table S4, Supporting Information), as required for two qubit systems (see above).

3. Conclusions and Perspectives

We have determined spin dynamics times for two mono- and one biradical perchlorinated triphenylmethyl radical derivatives in frozen solutions of nuclear-spin-free solvents and, we found them to be among the highest reported for paramagnetic molecules underlining their potential as molecular qubits. Furthermore, we have demonstrated and quantified the intramolecular spin-spin coupling in the biradical by microwave pulse sequences that ensure individual addressability of the two spin centers within the resonator bandwidth. Strikingly, this demonstrates their potential as two qubit systems. The single qubit figure of merit for these systems is of the order of 10^4 (for a coherence time of 100 μs and a manipulation time of 10 ns), even without dynamical decoupling techniques, which is competitive with state-of-the-art qubit platforms. We believe that the impact and importance of these results is the following:

1) Implementation of quantum algorithms: The ensemble coherence times of molecular one- and two-qubit systems are

**ADVANCED
SCIENCE NEWS**

www.advancedsciencenews.com

**ADVANCED
MATERIALS**

www.advmat.de

now of the order of 100 μs, which is sufficient to implement two-qubit gate operations at temperatures of the order of 100 K. Inclusion of dynamical decoupling can enhance coherence times by an order of magnitude.[10]

2) Molecular engineering: PTM-type radicals can be functionalized, allowing the preparation of larger more-qubit systems, deposition of these species on surfaces for device integration, or functionalization with receptor units for quantum sensing of analytes.[66]

3) Toward single quantum entity microwave readout: One of the main advantages of defect-center-based qubits, such as NV$^-$-centers in diamond is that they can be read out on a single-entity level at high temperatures. In molecular qubits, this has only been achieved (by electrical addressing) at millikelvin temperatures.[13] NV$^-$-centers only possess their favorable properties if they are located deep within (>10 nm) the diamond matrix, which is disadvantageous for quantum sensing of analytes. Developing trityl-NV hybrid systems may allow synergetic profiting from the advantages of both materials.

4) Toward single quantum entity optical readout: perchlorinated trityl radicals show photoluminescence by either the replacement of one of the chlorinated aryl groups for a 4-pyridyl group,[87] or by a proper isolation of these radicals in rigid matrices or on surfaces.[88] This may be a first step toward organic-radical based MQBs suitable for optical readout. The challenge here is to develop photostable, luminescent triplet-ground state biradicals.

4. Experimental Section

Materials: Carbon disulfide (CS_2), toluene and dichloromethane solvents as well as PSF polymer were obtained commercially. All solvents for EPR measurements were dried according to appropriate procedures.

Synthesis: PTM,[89] mPTM,[90] and bPTM[91] were synthesized and characterized as previously reported. Doped samples of mPTM in αH-mPTM were obtained by solution mixing followed by drop casting. Unfortunately, the lack of crystallinity prevents recording meaningful powder X-ray diffractograms for further characterization of doped and pristine samples (Figure S15, Supporting Information).

Pulsed Electron Paramagnetic Resonance: Pulsed electron paramagnetic resonance spectra were recorded on a home-built pulsed Q-band spectrometer, equipped with a TE011 cylindrical resonator and operating at 35.000 GHz.[92] Samples were dissolved into CS_2 solvent, freeze quenched and inserted into the precooled cavity. Phase memory times TM were determined by using the Hahn echo sequence $(\frac{\pi}{2}) - \tau - (\pi) - \tau - echo$, and spin–lattice relaxation times T_1 were determined by the inversion recovery sequence $(\pi) - T - (\frac{\pi}{2}) - \tau - (\pi) - \tau - echo$. The Hahn echo sequence was also used for recording echo-detected field-swept EPR spectra. Spectra were simulated using the EasySpin toolbox.[93] Relaxation data were analyzed by means of scripts written in Python 3.8 in the Spyder IDE 5.0.

Pulsed Dipolar EPR: Pulsed Dipolar EPR measurements were carried out on a Bruker Elexsys E580 FT spectrometer, equipped with a 3 mm Dual Mode Resonator (T2), an AWG pulse shaping unit, and a cryogenic cryogen-free cryostat enabling operations at low temperatures. Samples were dissolved into a 1:1 anhydrous mixture of toluene and dichloromethane, and freeze quenched and inserted into the precooled resonator. All m.w. pulses were optimized and amplified via a pulsed travelling wave tube amplifier. Data were processed and analyzed by means of the DeerAnalysis 2021b toolbox.[94,95]

Calculations: All calculations in this work were performed with the electronic structure program ORCA.[96] Geometry optimizations were carried out by DFT using the B3LYP functional in a vacuum.[97–100] A segmented all-electron relativistically contracted basis set of triple-ζ-quality (def2-TZVPP) was used for all atoms,[101] with Weigends general coulombic auxiliary basis set (def2/J) to expedite the calculations.[102] A dispersion correction was applied using Becke–Johnson damping.[103] The self-consistent field calculations were tightly converged (1×10^{-8} Eh in energy, 1×10^{-7} Eh in the density change, and 1×10^{-7} in the maximum element of the DIIS[104,105] error vector). The geometry search for all complexes was carried out in redundant internal coordinates without imposing geometry constraints. Geometry optimized structure plots were constructed using the program Avogadro2.[106]

Supporting Information

Supporting Information is available from the Wiley Online Library or from the author.

Conflict of Interest

The authors declare no conflict of interest.

Data Availability Statement

The data that support the findings of this study are available from the corresponding author upon reasonable request.

[1] J. S. Sidhu, S. K. Joshi, M. Gündoğan, T. Brougham, D. Lowndes, L. Mazzarella, M. Krutzik, S. Mohapatra, D. Dequal, G. Vallone, P. Villoresi, A. Ling, T. Jennewein, M. Mohageg, J. G. Rarity, I. Fuentes, S. Pirandola, D. K. L. Oi, *IET Quantum Commun.* **2021**, *2*, 182.

[2] https://newsroom.ibm.com/2022-11-09-IBM-Unveils-400-Qubit-Plus-Quantum-Processor-and-Next-Generation-IBM-Quantum-System-Two. Accessed 14 Nov **2022**

[3] J. F. Barry, M. J. Turner, J. M. Schloss, D. R. Glenn, Y. Song, M. D. Lukin, H. Park, R. L. Walsworth, *Proc. Natl. Acad. Sci. U. S. A.* **2016**, *113*, 14133.

[4] E. Janitz, K. Herb, L. A. Völker, W. S. Huxter, C. L. Degen, J. M. Abendroth, *J. Mater. Chem. C* **2022**, *10*, 13533.

[5] S. Pezzagna, D. Wildanger, P. Mazarov, A. D. Wieck, Y. Sarov, I. Rangelow, B. Naydenov, F. Jelezko, S. W. Hell, J. Meijer, *Small* **2010**, *6*, 2117.

[6] J. Ferrando-Soria, *Magnetochemistry* **2016**, *2*, 36.

[7] S. Zhou, J. Yuan, Z.-Y. Wang, K. Ling, P.-X. Fu, Y.-H. Fang, Y.-X. Wang, Z. Liu, K. Porfyrakis, G. A. D. Briggs, S. Gao, S.-D. Jiang, *Angew. Chem., Int. Ed.* **2022**, *61*, e202115263.

[8] C.-J. Yu, M. D. Krzyaniak, M. S. Fataftah, M. R. Wasielewski, D. E. Freedman, *Chem. Sci.* **2019**, *10*, 1702.

[9] A. Urtizberea, E. Natividad, P. J. Alonso, M. A. Andrés, I. Gascón, M. Goldmann, O. Roubeau, *Adv. Funct. Mater.* **2018**, *28*, 1801695.

[10] Y. Dai, Y. Fu, Z. Shi, X. Qin, S. Mu, Y. Wu, J.-H. Su, Y.-F. Deng, L. Qin, Y.-Q. Zhai, Y.-Z. Zheng, X. Rong, J. Du, *Chin. Phys. Lett.* **2021**, *38*, 030303.

[11] J. M. Zadrozny, J. Niklas, O. G. Poluektov, D. E. Freedman, *ACS Cent. Sci.* **2015**, *1*, 488.

[12] M. Warner, S. Din, I. S. Tupitsyn, G. W. Morley, A. M. Stoneham, J. A. Gardener, Z. Wu, A. J. Fisher, S. Heutz, C. W. M. Kay, G. Aeppli, *Nature* **2013**, *503*, 504.

[13] S. Thiele, F. Balestro, R. Ballou, S. Klyatskaya, M. Ruben, W. Wernsdorfer, *Science* **2014**, *344*, 1135.

[14] S. von Kugelgen, M. D. Krzyaniak, M. Gu, D. Puggioni, J. M. Rondinelli, M. R. Wasielewski, D. E. Freedman, *J. Am. Chem. Soc.* **2021**, *143*, 8069.

[15] D. Serrano, S. K. Kuppusamy, B. Heinrich, O. Fuhr, D. Hunger, M. Ruben, P. Goldner, *Nature* **2022**, *603*, 241.

[16] D. Aguila, L. A. Barrios, V. Velasco, O. Roubeau, A. Repolles, P. J. Alonso, J. Sese, S. J. Teat, F. Luis, G. Aromi, *J. Am. Chem. Soc.* **2014**, *136*, 14215.

[17] E. Macaluso, M. Rubín, D. Aguilà, A. Chiesa, L. A. Barrios, J. I. Martínez, P. J. Alonso, O. Roubeau, F. Luis, G. Aromí, S. Carretta, *Chem. Sci.* **2020**, *11*, 10337.

[18] L. M. K. Vandersypen, I. L. Chuang, *Rev. Mod. Phys.* **2005**, *76*, 1037.

[19] S. Nakazawa, S. Nishida, T. Ise, T. Yoshino, N. Mori, R. D. Rahimi, K. Sato, Y. Morita, K. Toyota, D. Shiomi, M. Kitagawa, H. Hara, P. Carl, P. Höfer, T. Takui, *Angew. Chem., Int. Ed.* **2012**, *51*, 9860.

[20] A. Ardavan, A. M. Bowen, A. Fernandez, A. J. Fielding, D. Kaminski, F. Moro, C. A. Muryn, M. D. Wise, A. Ruggi, E. J. L. McInnes, K. Severin, G. A. Timco, C. R. Timmel, F. Tuna, G. F. S. Whitehead, R. E. P. Winpenny, *npj Quantum Inf.* **2015**, *1*, 15012.

[21] D. Abdullin, O. Schiemann, *ChemPlusChem* **2020**, *85*, 353.

[22] S. Valera, B. E. Bode, *Molecules* **2014**, *19*, 20227.

[23] G. Jeschke, *ChemPhysChem* **2002**, *3*, 927.

[24] K. Bader, D. Dengler, S. Lenz, B. Endeward, S.-D. Jiang, P. Neugebauer, J. van Slageren, *Nat. Commun.* **2014**, *5*, 5304.

[25] W. Harneit, in *Endohedral Fullerenes: Electron Transfer and Spin* (Ed.: A. A. Popov), Springer, Cham **2017**, pp. 297–324.

[26] P. Jakes, K.-P. Dinse, C. Meyer, W. Harneit, A. Weidinger, *Phys. Chem. Chem. Phys.* **2003**, *5*, 4080.

[27] B. J. Farrington, M. Jevric, G. A. Rance, A. Ardavan, A. N. Khlobystov, G. A. D. Briggs, K. Porfyrakis, *Angew. Chem., Int. Ed.* **2012**, *51*, 3587.

[28] O. Schiemann, C. A. Heubach, D. Abdullin, K. Ackermann, M. Azarkh, E. G. Bagryanskaya, M. Drescher, B. Endeward, J. H. Freed, L. Galazzo, D. Goldfarb, T. Hett, L. Esteban Hofer, L. Fábregas Ibáñez, E. J. Hustedt, S. Kucher, I. Kuprov, J. E. Lovett, A. Meyer, S. Ruthstein, S. Saxena, S. Stoll, C. R. Timmel, M. Di Valentin, H. S. McHaourab, T. F. Prisner, B. E. Bode, E. Bordignon, M. Bennati, G. Jeschke, *J. Am. Chem. Soc.* **2021**, *143*, 17875.

[29] Y.-Z. Dai, B.-W. Dong, Y. Kao, Z.-Y. Wang, H.-I. Un, Z. Liu, Z.-J. Lin, L. Li, F.-B. Xie, Y. Lu, M.-X. Xu, T. Lei, Y.-J. Sun, J.-Y. Wang, S. Gao, S.-D. Jiang, J. Pei, *ChemPhysChem* **2018**, *19*, 2972.

[30] F. Lombardi, A. Lodi, J. Ma, J. Liu, M. Slota, A. Narita, W. K. Myers, K. Müllen, X. Feng, L. Bogani, *Science* **2019**, *366*, 1107.

[31] J. J. L. Morton, A. M. Tyryshkin, A. Ardavan, K. Porfyrakis, S. A. Lyon, G. A. D. Briggs, *Phys. Rev. B* **2007**, *76*, 085418.

[32] K. Bader, M. Winkler, J. van Slageren, *Chem. Commun.* **2016**, *52*, 3623.

[33] L. C. de Camargo, M. Briganti, F. S. Santana, D. Stinghen, R. R. Ribeiro, G. G. Nunes, J. F. Soares, E. Salvadori, M. Chiesa, S. Benci, R. Torre, L. Sorace, F. Totti, R. Sessoli, *Angew. Chem., Int. Ed.* **2021**, *60*, 2588.

[34] S. Lenz, K. Bader, H. Bamberger, J. van Slageren, *Chem. Commun.* **2017**, *53*, 4477.

[35] J. McGuire, H. N. Miras, E. Richards, S. Sproules, *Chem. Sci.* **2019**, *10*, 1483.

[36] L. Tesi, F. Stemmler, M. Winkler, S. S. Y. Liu, S. Das, X. Sun, M. Zharnikov, S. Ludwigs, J. van Slageren, *Adv. Mater.* **2023**, *35*, 2208998.

[37] A. S. Poryvaev, E. Gjuzi, D. M. Polyukhov, F. Hoffmann, M. Fröba, M. V. Fedin, *Angew. Chem., Int. Ed.* **2021**, *60*, 8683.

[38] O. A. Krumkacheva, I. O. Timofeev, L. V. Politanskaya, Y. F. Polienko, E. V. Tretyakov, O. Y. Rogozhnikova, D. V. Trukhin, V. M. Tormyshev, A. S. Chubarov, E. G. Bagryanskaya, M. V. Fedin, *Angew. Chem., Int. Ed.* **2019**, *58*, 13271.

[39] A. Collauto, M. Mannini, L. Sorace, A. Barbon, M. Brustolon, D. Gatteschi, *J. Mater. Chem.* **2012**, *22*, 22272.

[40] A. J. Fielding, P. J. Carl, G. R. Eaton, S. S. Eaton, *Appl. Magn. Reson.* **2005**, *28*, 231.

[41] V. Meyer, S. S. Eaton, G. R. Eaton, *Appl. Magn. Reson.* **2013**, *44*, 509.

[42] A. Rajca, V. Kathirvelu, S. K. Roy, M. Pink, S. Rajca, S. Sarkar, S. S. Eaton, G. R. Eaton, *Chem. - Eur. J.* **2010**, *16*, 5778.

[43] C. Bonizzoni, M. Maksutoglu, A. Ghirri, J. van Tol, B. Rameev, M. Affronte, *Appl. Magn. Reson.* **2022**, https://doi.org/10.1007/s00723-022-01505-8.

[44] J. S. Uber, M. Estrader, J. Garcia, P. Lloyd-Williams, A. Sadurní, D. Dengler, J. van Slageren, N. F. Chilton, O. Roubeau, S. J. Teat, J. Ribas-Ariño, G. Aromí, *Chem. - Eur. J.* **2017**, *23*, 13648.

[45] D. Ranieri, F. Santanni, A. Privitera, A. Albino, E. Salvadori, M. Chiesa, F. Totti, L. Sorace, R. Sessoli, *Chem. Sci.* **2023**, *14*, 61.

[46] I. Pozo, F. Lombardi, D. Alexandropoulos, F. Kong, J.-R. Deng, P. Horton, S. Coles, W. Myers, L. Bogani, H. Anderson, *ChemRxiv* **2023**. 10.26434/chemrxiv-22022-26431v26435b26434.

[47] D. Akhmetzyanov, H. Y. V. Ching, V. Denysenkov, P. Demay-Drouhard, H. C. Bertrand, L. C. Tabares, C. Policar, T. F. Prisner, S. Un, *Phys. Chem. Chem. Phys.* **2016**, *18*, 30857.

[48] W. Moore, R. Yao, Y. Liu, S. S. Eaton, G. R. Eaton, *J. Magn. Reson.* **2021**, *332*, 107078.

[49] N. Wili, H. Hintz, A. Vanas, A. Godt, G. Jeschke, *Magn. Reson.* **2020**, *1*, 75.

[50] G. Gil-Ramírez, A. Shah, H. El Mkami, K. Porfyrakis, G. A. D. Briggs, J. J. L. Morton, H. L. Anderson, J. E. Lovett, *J. Am. Chem. Soc.* **2018**, *140*, 7420.

[51] M. Azarkh, A. Bieber, M. Qi, J. W. A. Fischer, M. Yulikov, A. Godt, M. Drescher, *J. Phys. Chem. Lett.* **2019**, *10*, 1477.

[52] D. Akhmetzyanov, J. Plackmeyer, B. Endeward, V. Denysenkov, T. F. Prisner, *Phys. Chem. Chem. Phys.* **2015**, *17*, 6760.

[53] M. Atzori, A. Chiesa, E. Morra, M. Chiesa, L. Sorace, S. Carretta, R. Sessoli, *Chem. Sci.* **2018**, *9*, 6183.

[54] A. Fernandez, E. Moreno Pineda, C. A. Muryn, S. Sproules, F. Moro, G. A. Timco, E. J. L. McInnes, R. E. P. Winpenny, *Angew. Chem., Int. Ed.* **2015**, *54*, 10858.

[55] I. Borilovic, P. J. Alonso, O. Roubeau, G. Aromí, *Chem. Commun.* **2020**, *56*, 3139.

[56] D. Banerjee, J. C. Paniagua, V. Mugnaini, J. Veciana, A. Feintuch, M. Pons, D. Goldfarb, *Phys. Chem. Chem. Phys.* **2011**, *13*, 18626.

[57] J. C. Paniagua, V. Mugnaini, C. Gabellieri, M. Feliz, N. Roques, J. Veciana, M. Pons, *Phys. Chem. Chem. Phys.* **2010**, *12*, 5824.

[58] F. Graf, K. Loth, H.-H. Günthard, *Helv. Chim. Acta* **1977**, *60*, 710.

[59] W. Moore, J. L. Huffman, B. Driesschaert, S. S. Eaton, G. R. Eaton, *Appl. Magn. Reson.* **2022**, *53*, 797.

[60] J. L. Huffman, M. Poncelet, W. Moore, S. S. Eaton, G. R. Eaton, B. Driesschaert, *J. Phys. Chem. B* **2021**, *125*, 7380.

[61] A. Boś-Liedke, M. Walawender, A. Woźniak, D. Flak, J. Gapiński, S. Jurga, M. Kucińska, A. Plewiński, M. Murias, M. Elewa, L. Lampp, P. Imming, K. Tadyszak, *Cell Biochem.* **2018**, *76*, 19.

[62] P. Demay-Drouhard, H. Y. V. Ching, C. Decroos, R. Guillot, Y. Li, L. C. Tabares, C. Policar, H. C. Bertrand, S. Un, *Phys. Chem. Chem. Phys.* **2020**, *22*, 20792.

[63] F. M. Vigier, D. Shimon, V. Mugnaini, J. Veciana, A. Feintuch, M. Pons, S. Vega, D. Goldfarb, *Phys. Chem. Chem. Phys.* **2014**, *16*, 19218.

[64] M. Poncelet, J. L. Huffman, V. V. Khramtsov, I. Dhimitruka, B. Driesschaert, *RSC Adv.* **2019**, *9*, 35073.

[65] S. Takahashi, J. van Tol, C. C. Beedle, D. N. Hendrickson, L.-C. Brunel, M. S. Sherwin, *Phys. Rev. Lett.* **2009**, *102*, 087603.

[66] J. A. de Sousa, F. Bejarano, D. Gutiérrez, Y. R. Leroux, E. M. Nowik-Boltyk, T. Junghoefer, E. Giangrisostomi, R. Ovsyannikov, M. B. Casu, J. Veciana, M. Mas-Torrent, B. Fabre, C. Rovira, N. Crivillers, *Chem. Sci.* **2020**, *11*, 516.

[67] G. Balasubramanian, P. Neumann, D. Twitchen, M. Markham, R. Kolesov, N. Mizuochi, J. Isoya, J. Achard, J. Beck, J. Tissler, V. Jacques, P. R. Hemmer, F. Jelezko, J. Wrachtrup, *Nat. Mater.* **2009**, *8*, 383.

[68] M. Atzori, S. Benci, E. Morra, L. Tesi, M. Chiesa, R. Torre, L. Sorace, R. Sessoli, *Inorg. Chem.* **2018**, *57*, 731.

[69] L. Tesi, E. Lucaccini, I. Cimatti, M. Perfetti, M. Mannini, M. Atzori, E. Morra, M. Chiesa, A. Caneschi, L. Sorace, R. Sessoli, *Chem. Sci.* **2016**, *7*, 2074.

[70] A. Abragam, B. Bleany, *Electron Paramagnetic Resonance of Transition Ions*, Dover Publications, Inc., New York **1986**.

[71] K. N. Shrivastava, *Phys. Status Solidi (B)* **1983**, *117*, 437.

[72] H. J. Jodl, M. Jordan, H. Däufer, *J. Chem. Phys.* **1993**, *98*, 2332.

[73] L. Tesi, A. Lunghi, M. Atzori, E. Lucaccini, L. Sorace, F. Totti, R. Sessoli, *Dalton Trans.* **2016**, *45*, 16635.

[74] S. K. Hoffmann, J. Goslar, *J. Phys.: Condens. Matter* **2015**, *27*, 265402.

[75] A. Lunghi, *arXiv:2202.03776* **2022**.

[76] J. G. Castle, D. W. Feldman, P. G. Klemens, R. A. Weeks, *Phys. Rev.* **1963**, *130*, 577.

[77] S. K. Hoffmann, S. Lijewski, *J. Magn. Reson.* **2013**, *227*, 51.

[78] V. Kathirvelu, G. R. Eaton, S. S. Eaton, *Appl. Magn. Reson.* **2009**, *37*, 649.

[79] C. J. Rogers, D. Asthana, A. Brookfield, A. Chiesa, G. A. Timco, D. Collison, L. S. Natrajan, S. Carretta, R. E. P. Winpenny, A. M. Bowen, *Angew. Chem., Int. Ed.* **2022**, *61*, e202207947.

[80] A. Meyer, J. J. Jassoy, S. Spicher, A. Berndhäuser, O. Schiemann, *Phys. Chem. Chem. Phys.* **2018**, *20*, 13858.

[81] G. Jeschke, M. Pannier, A. Godt, H. W. Spiess, *Chem. Phys. Lett.* **2000**, *331*, 243.

[82] N. C. Kunjir, G. W. Reginsson, O. Schiemann, S. T. Sigurdsson, *Phys. Chem. Chem. Phys.* **2013**, *15*, 19673.

[83] P. Schöps, P. E. Spindler, A. Marko, T. F. Prisner, *J. Magn. Reson.* **2015**, *250*, 55.

[84] P. P. Borbat, J. H. Freed, in *eMagRes* (Eds.: R. K. Harris, R. L. Wasylishen), Wiley, New York **2017**, pp. 465–494.

[85] A. Schweiger, G. Jeschke, *Principles of Pulse Electron Paramagnetic Resonance*, Oxford University Press, Oxford **2001**.

[86] G. Jeschke, in *eMagRes* (Eds.: R. K. Harris, R. L. Wasylishen), **2016**, pp. 1459–1476.

[87] Y. Hattori, T. Kusamoto, H. Nishihara, *Angew. Chem., Int. Ed.* **2014**, *53*, 11845.

[88] D. Blasi, D. M. Nikolaidou, F. Terenziani, I. Ratera, J. Veciana, *Phys. Chem. Chem. Phys.* **2017**, *19*, 9313.

[89] M. Ballester, J. Riera-Figueras, J. Castaner, C. Badfa, J. M. Monso, *J. Am. Chem. Soc.* **1971**, *93*, 2215.

[90] F. Bejarano, I. J. Olavarria-Contreras, A. Droghetti, I. Rungger, A. Rudnev, D. Gutiérrez, M. Mas-Torrent, J. Veciana, H. S. J. van der Zant, C. Rovira, E. Burzurı́, N. Crivillers, *J. Am. Chem. Soc.* **2018**, *140*, 1691.

[91] P. Mayorga-Burrezo, F. Bejarano, J. Calbo, X. Zhao, J. A. De Sousa, V. Lloveras, M. R. Bryce, E. Ortí, J. Veciana, C. Rovira, N. Crivillers, *J. Phys. Chem. Lett.* **2021**, *12*, 6159.

[92] I. Tkach, A. Baldansuren, E. Kalabukhova, S. Lukin, A. Sitnikov, A. Tsvir, M. Ischenko, Y. Rosentzweig, E. Roduner, *Appl. Magn. Reson.* **2008**, *35*, 95.

[93] S. Stoll, A. Schweiger, *J. Magn. Reson.* **2006**, *178*, 42.

[94] G. Jeschke, DeerAnalysis 2021b, ETH Zürich, **2021**.

[95] G. Jeschke, V. Chechik, P. Ionita, A. Godt, H. Zimmermann, J. Banham, C. R. Timmel, D. Hilger, H. Jung, *Appl. Magn. Reson.* **2006**, *30*, 473.

[96] F. Neese, *Wiley Interdiscip. Rev. Comput. Mol. Sci.* **2012**, *2*, 73.

[97] S. H. Vosko, L. Wilk, M. Nusair, *Can. J. Phys.* **1980**, *58*, 1200.

[98] P. J. Stephens, F. J. Devlin, C. F. Chabalowski, M. J. Frisch, *J. Phys. Chem.* **1994**, *98*, 11623.

[99] C. Lee, W. Yang, R. G. Parr, *Phys. Rev. B* **1988**, *37*, 785.

[100] A. D. Becke, *J. Chem. Phys.* **1993**, *98*, 5648.

[101] D. A. Pantazis, X.-Y. Chen, C. R. Landis, F. Neese, *J. Chem. Theory Comput.* **2008**, *4*, 908.

[102] F. Weigend, *Phys. Chem. Chem. Phys.* **2006**, *8*, 1057.

[103] S. Grimme, S. Ehrlich, L. Goerigk, *J. Comput. Chem.* **2011**, *32*, 1456.

[104] P. Pulay, *J. Comput. Chem.* **1982**, *3*, 556.

[105] P. Pulay, *Chem. Phys. Lett.* **1980**, *73*, 393.

[106] M. D. Hanwell, D. E. Curtis, D. C. Lonie, T. Vandermeersch, E. Zurek, G. R. Hutchison, *J. Cheminform.* **2012**, *4*, 17.